IEEE Photonics Journal
An IEEE Photonics Society Publication

Open Access

Hollow-Core-Fiber-Based Interferometer for High-Temperature Measurements

Volume 9, Number 2, April 2017

Zhe Zhang
Changrui Liao
Jian Tang
Ying Wang
Zhiyong Bai
Zhengyong Li
Kuikui Guo
Mi Deng
Shaoqing Cao
Yiping Wang, *Senior Member, IEEE*

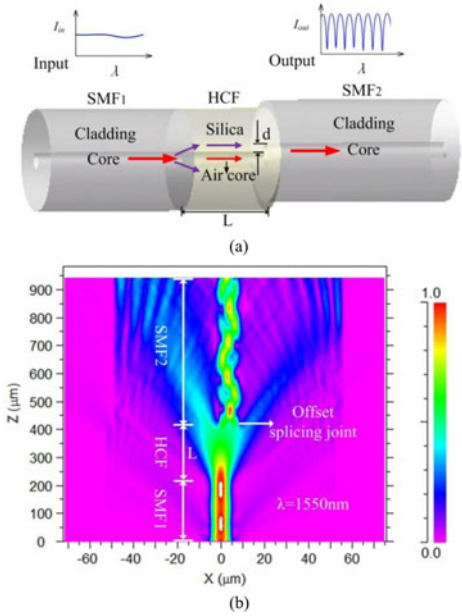

DOI: 10.1109/JPHOT.2017.2671437
1943-0655 © 2017 IEEE

Hollow-Core-Fiber-Based Interferometer for High-Temperature Measurements

Zhe Zhang, Changrui Liao, Jian Tang, Ying Wang, Zhiyong Bai, Zhengyong Li, Kuikui Guo, Mi Deng, Shaoqing Cao, and Yiping Wang, *Senior Member, IEEE*

Key Laboratory of Optoelectronic Devices and Systems of Ministry of Education, College of Optoelectronic Engineering, Shenzhen University, Shenzhen 518060, China

DOI:10.1109/JPHOT.2017.2671437
1943-0655 © 2017 IEEE. Translations and content mining are permitted for academic research only. Personal use is also permitted, but republication/redistribution requires IEEE permission. See http://www.ieee.org/publications_standards/publications/rights/index.html for more information.

Manuscript received December 22, 2016; revised February 9, 2017; accepted February 15, 2017. Date of publication February 23, 2017; date of current version March 7, 2017. This work was supported in part by the National Natural Science Foundation of China under Grant 61635007, Grant 61425007, Grant 61575128, and Grant 61405128; in part by the Guangdong Provincial Department of Science and Technology under Grant 2014A030308007, Grant 2014B050504010, Grant 2015B010105007, and Grant 2015A030313541; in part by the Science and Technology Innovation Commission of Shenzhen under Grant GJHZ20150313093755757, Grant JCYJ20160520163134575, Grant JCYJ20160427104925452, and Grant JCYJ2015032414171161; in part by the China Postdoctoral Science Foundation Funded Project under Grant 2015M572351 and Grant 2016T90796; and in part by the Pearl River Scholar Fellowships. Corresponding author: C. Liao (e-mail: cliao@szu.edu.cn).

Abstract: We report a new fiber optic sensor for temperature measurement at a temperature range of up to 900 °C with excellent stability and repeatability. The sensing head is comprised of a short hollow-core fiber segment spliced between two single-mode fibers using a commercial splicer. Optical power from the lead-in fiber is partly coupled to silica cladding of the hollow-core fiber with the remainder propagating in air core by short distance. The two beams are then re-coupled to the core of the lead-out fiber, owing to the offset splicing joint. Due to the effective index difference between the two beams, an interference pattern in the transmission spectrum is obtained. The distinct thermo-optic coefficients between silica and air result in a high-temperature sensitivity of 41 pm/ °C, and the enclosed structure ensures its immunity to the external refractive index.

Index Terms: Hollow-core fiber, interferometer, temperature sensor.

1. Introduction

Temperature measurement based on optical fiber devices has been extensively investigated due to their superior properties such as compact size, light weight, and easy for network use [1], [2]. Among them, fiber Bragg gratings (FBGs) and long-period fiber gratings (LPFGs) have been widely investigated for temperature sensing applications. Although FBG temperature sensors are attractive for distributed sensing, they have some disadvantages. Type I FBGs based on photosensitivity will be degenerated at a temperature higher than 350 °C [3]–[5]. Type II FBGs can work at a temperature up to 1000 °C, but its fabrication requires expensive high power lasers such as femtosecond laser or excimer laser [6]–[9]. Comparing with FBGs, LPFGs exhibit much higher temperature sensitivity [10]–[14], but their cross-sensitivity to external refractive index (RI) cannot be overcome [15]–[18].

Alternatively, fiber in-line interferometric sensors have been considered as good candidates for high-temperature sensors which exhibit high-temperature resistance and simultaneous high

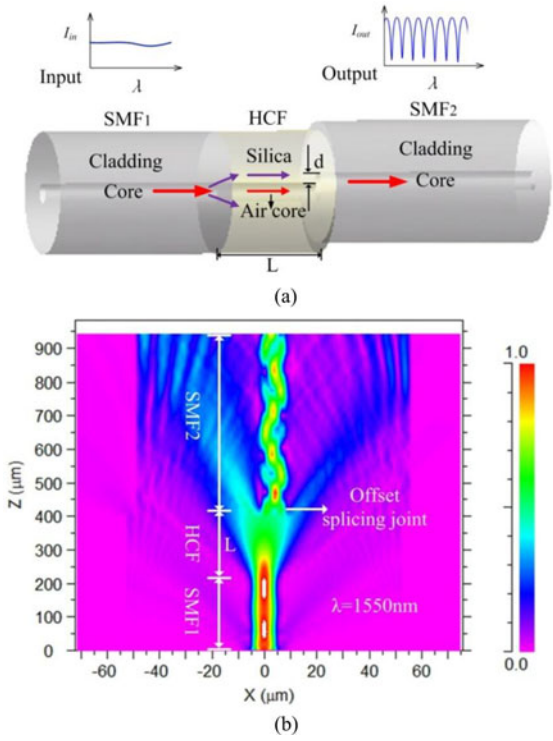

Fig. 1. (a) Schematic diagram of the proposed SMF-HCF-SMF temperature sensor. (b) Simulation result of light propagation in SMF-HCF-SMF configuration at 1550 nm.

sensitivity. Among them, multimode-fiber-based interferometer exhibits a relatively low temperature sensitivity of ~ 10 pm/ °C [19]–[21] due to the similar thermal-optic coefficient of the materials of the two interferometry beams. The larger difference between the thermal-optic coefficients, the higher sensitivity can be obtained [22]–[24]. The fiber Mach-Zehnder interferometer based on femtosecond-laser drilling hole can achieve a higher temperature sensitivity due to the distinct thermal-optic coefficients between air-hole and Ge-doped core, but the open hole of the sensor will introduce apparent cross-sensitivity to external RI [22], [23]. Moreover, Hollow-core fiber (HCF) with a high quality air core and enclosed structure makes it an excellent candidate for optical fiber interferometric temperature sensors. The silica cladding of HCF can sustain a temperature higher than 1000 °C, and the air core provides an excellent optical path.

In this paper, we demonstrate an environmental RI insensitive high-temperature sensor comprised of a short HCF segment spliced between two SMFs using a commercial splicer, and employs a working principle based on interference between the core and cladding beams of the HCF. The simple architecture of the sensor does not yield an excellent performance. Systematical high-temperature test has been carried out and a high temperature sensitivity of 41 pm/ °C, and an excellent high temperature stability up to 900 °C has been achieved. The sensor with enclosed structure is immune to external RI, which may be vital in hyperthermal liquid temperature monitor.

2. Working Principle

Fig. 1(a) schematically illustrates the structure of the proposed sensor. The light propagating in SMF_1 will divided into two components at the first aligned joint, and a fraction of light will propagate into the silica cladding of HCF as Cladding Beam while the majority of light will propagate through the air core of HCF as Core Beam when the HCF is short enough. The light propagation in SMF-HCF-SMF configuration is simulated by use of beam propagation method (BPM), and the result is shown in Fig. 1(b). From Fig. 1(b), it can seen that the light is split at the left aligned joint, and after

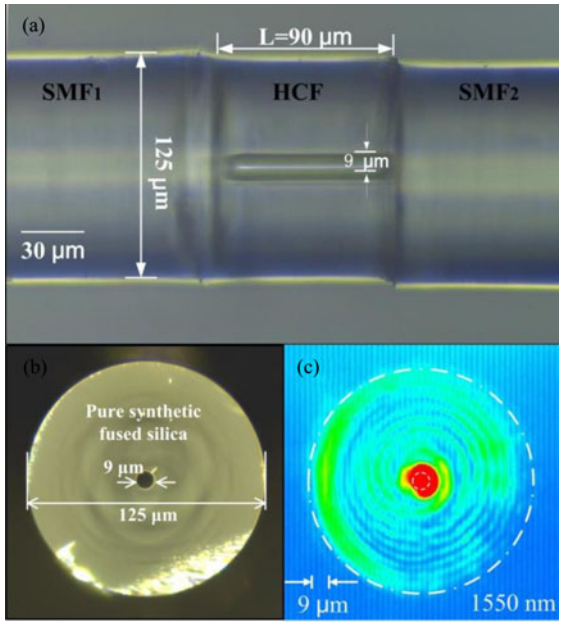

Fig. 2. (a) Side view of the sensing head. (b) Cross section of the HCF. (c) Near field image at the endfacet of a 90 μm HCF with the other endfacet aligned to the lead-in SMF_1.

propagating through the HCF, the Cladding Beam and Core Beam are recombined in SMF_2 at the right joint with an offset distance d. The interference pattern can be observed in the transmission spectrum due to the optical path difference (OPD) between the two beams. Denoting the optical intensity of the cladding and core beams recombined into SMF_2 as I_{out1} and I_{out2}, respectively, the total output intensity can be expressed as

$$I = I_{co} + I_{cl} + 2\sqrt{I_{co} I_{cl}} \cos\left(\frac{2\pi L\,\Delta n}{\lambda} + \varphi_0\right) \tag{1}$$

where λ is the light wavelength, L is the length of HCF, $\Delta n = n_{cl}^{eff} - n_{co}^{eff}$ is the effective RI difference between the two interference beams, n_{cl}^{eff} *and* n_{co}^{eff} represent for the effective RIs of Cladding Beam and Core Beam, respectively, and φ_0 is the initial phase of interference. According to (1), the interference signal attains a minimum value when the following condition is satisfied:

$$\frac{2\pi L\,\Delta n}{\lambda_m} + \varphi_0 = (2m+1)\pi \tag{2}$$

where m is an integer and λ_m is the wavelength of the m^{th} order interference minimum. The free spectral range (FSR) of this fiber interferometer can be expressed as

$$\mathrm{FSR} = \frac{\lambda^2}{\Delta n L} \tag{3}$$

the wavelength of the m^{th} order interference minimum can be express as

$$\lambda_m = \frac{2\pi L\,\Delta n}{(2m+1)\pi - \varphi_0}. \tag{4}$$

3. Sensor Fabrication

The air-core diameter of the employed HCF is 9 μm, which is shown in Fig. 2(b). The left end of HCF is spliced to SMF_1 with no offset working as a beam splitter while the right end is spliced to

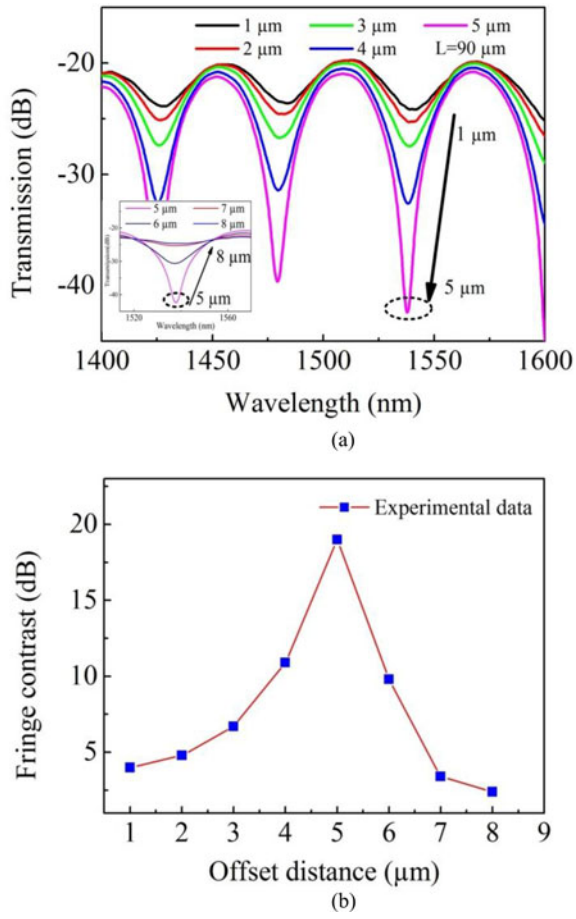

Fig. 3. (a) Transmission spectra for different offset distances. (Inset) Transmission spectrum shrink. (b) Fringe contrast versus offset distance.

SMF_2 with an optimized offset working as a beam combiner. During the fabrication, a broadband light source (BBS) and an optical spectral analyzer (OSA) are employed to monitor its spectrum online. The offset distance between HCF and SMF_2 plays a key role to optimize the spectrum. The translation step of the used fusion splicer in the direction perpendicular to fiber axis is 1 μm that is good enough to precisely control the offset distance aiming to achieve good interference spectrum. Fig. 2(a) is an optical microscope image of the sensor containing a section of HCF with a length of 90 μm. Fig. 2(c) is the near field image at the right end of HCF recorded by use of an infrared camera and a wavelength tunable laser. Fig. 3(a) presents the transmission spectra of SMF-HCF-SMF configuration with different offset distance and the relationship between fringe visibility and offset distance is illustrated in Fig. 3(b), where the fringe visibility reaches the peak value of $\sim$18 dB with the offset distance being 5 μm. The coupling behavior (fringe contrast) with regard to the offset can be understand from Fig. 2(c), where the intensity of the two interference beams becomes approximately equal with an offset distance of $\sim$5 μm.

From (3), the FSR is inversely proportional to L and therefore the FSR can be optimized by adjusting L for a given λ. To experimentally study the relationship between FSR and L, four samples with different HCF length of 90, 105, 160, and 190 μm have been fabricated and their transmission spectra are measured at room temperature (25 °C), which are shown in Fig. 4(a) and the FSR values of the four samples at 1550 nm are measured and denoted by the red squares in Fig. 4(b). Assuming $n_{si}^{eff} = 1.445$, $n_{air}^{eff} = 1.000$ (at 1550 nm), according to (3), the calculated relationship

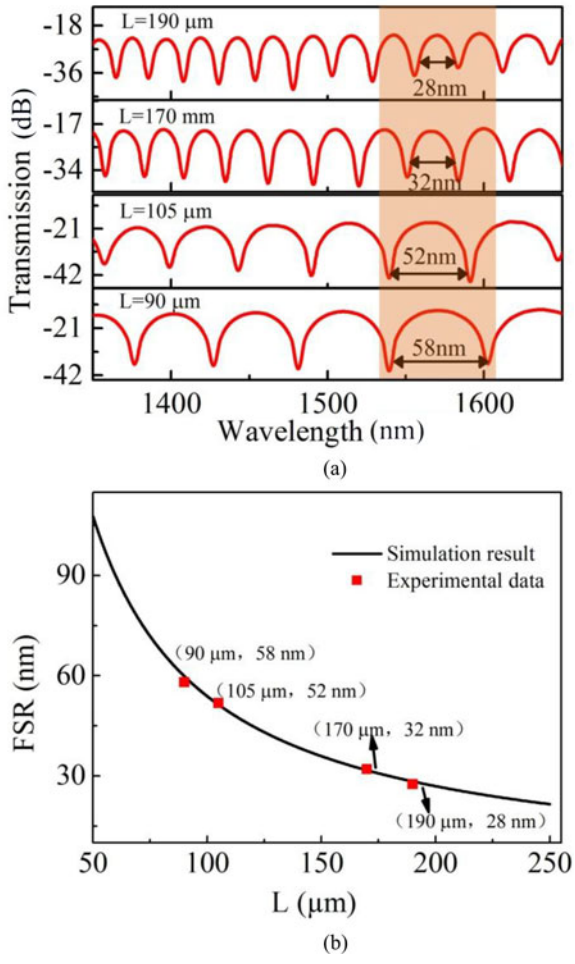

Fig. 4. (a) Measured transmission spectra at room temperature with different HCF length L of 190 μm, 170 μm, 105 μm, and 90 μm. (b) Measured and calculated FSR values of the interference fringes shown in Fig. 4(a).

between FSR and L is plotted by the black line in Fig. 4(b), and the experimental result agrees well with the calculate one.

4. Sensing Performance Test

Temperature response test has been performed in a high-temperature oven (Carbolite 301), which can reach 1200 °C with an accuracy of ±1 °C. Fig. 5 illustrates the schematic diagram of the experimental setup, where a broadband light source (BBS) and optical spectral analyzer are again employed to monitor the spectrum in real time. The interference dip positioned around 1375 nm has been tracked in temperature sensing because it exhibits a pronounced fringe visibility in the experiment. The ambient temperature is increased from 200 °C to 900 °C with a step of 100 °C, and kept at each designated temperature for ~30mins to record a stable spectrum. The tract dip is shifted towards the longer wavelength with temperature increasing as shown in Fig. 6(a). Then the temperature is kept at 900 °C for 26 h, there is no obvious deterioration of the spectrum, and the tracked dip shifts by only 1.4 nm, as shown in Fig. 6(b). We believe that the tracked dip shift may result from residual stress release of the HCF. Then the temperature is decreased back to 200 °C with a step of 100 °C, and the spectral evolution is shown in Fig. 6(c). Note that the spectrum of

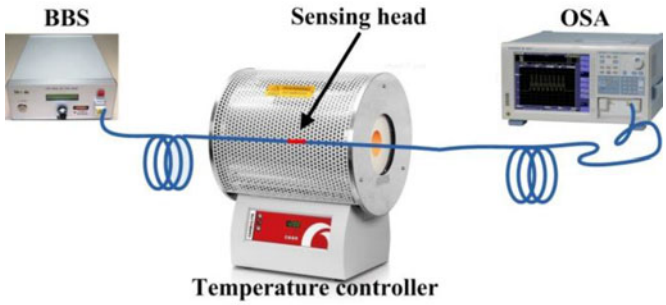

Fig. 5. Schematic diagram of the experimental setup for temperature tests.

Fig. 6(c) is tightly different from that of Fig. 6(a), the later one looks like having higher-order terms. In high temperature test, the refractive index profile of HCF may be modified due to the residual stress release of HCF and thus some new cladding modes in HCF can be excited and take part in interference. The plot of indicated wavelength versus temperature in both heating and cooling process are illustrated in Fig. 7(a), respectively. After repeating the heating and cooling cycles three times over 2 days, the tracked dip exhibits a good agreement in heating and cooling process as shown in Fig. 7(b), which confirms the sensor has a good repeatability and stability. The linear fitting yields a high correlation coefficient $R^2 = 0.9994$ and temperature sensitivity of 41pm/ °C.

RI response of this device has been also investigated. It was immersed in a series of RI liquids (Cargille Labs) in the range from 1.400 to 1.700 with an interval of 0.06 and then carefully cleaned by use of alcohol to completely remove any residual liquid. A new round test can be carried out when the spectrum return to the initial state in air. The result is that the spectrum is hardly changed in liquid environment.

5. Discussions

Due to the distinct thermo-optic coefficients between silica [25] and air, the difference of effective index between silica and air Δ n increase when temperature rise. Therefore, according to (4), λ_m will shift to longer wavelength with the temperature being increased.

Equation (4) indicates that the wavelength of fringe dips is related to HCF length and the effective index difference between Cladding Beam and Core Beam. We make differentiation for (4). Therefore, the temperature sensitivity can be calculated as

$$\frac{d\lambda}{dT} = \lambda \left[\frac{1}{n_{si}^{eff}(T) - n_{air}^{eff}(T)} \left(\frac{dn_{si}^{eff}(T)}{dT} - \frac{dn_{air}^{eff}(T)}{dT} \right) + \alpha \right] \tag{5}$$

where $n_{si}^{eff}(T)$ and $n_{air}^{eff}(T)$ are functions of temperature, α is thermal expansion coefficient of silica, and $dn_{si}^{eff}(T)/dT$, $dn_{air}^{eff}(T)/dT$ are thermo-optic coefficient of silica and air, respectively. The experimental measured thermo-optic coefficient of pure fused silica at different temperature range from 26 °C to 828 °C at some typical wavelength is illustrated in Table I [25].

From Table I, we can see that the thermo-optic coefficient of fused silica is higher than 10^{-5}. For pure fused silica [26], the thermal expansion coefficient is about 0.55×10^{-6}/ °C, which may contributes little to the wavelength shift according to (5). The RI of air can be expressed as

$$n = 1 + \frac{2.8793 \times 10^{-9} P}{1 + 0.003671 \times T} \tag{6}$$

where P and T are pressure and temperature. Considering the gas in HCF as ideal gas, according to the Ideal-gas equation PV = n R T, the RI of air is hardly changed. For simplification, we neglect the RI variation of air in calculation. According to the parameters above, the temperature-sensitivity

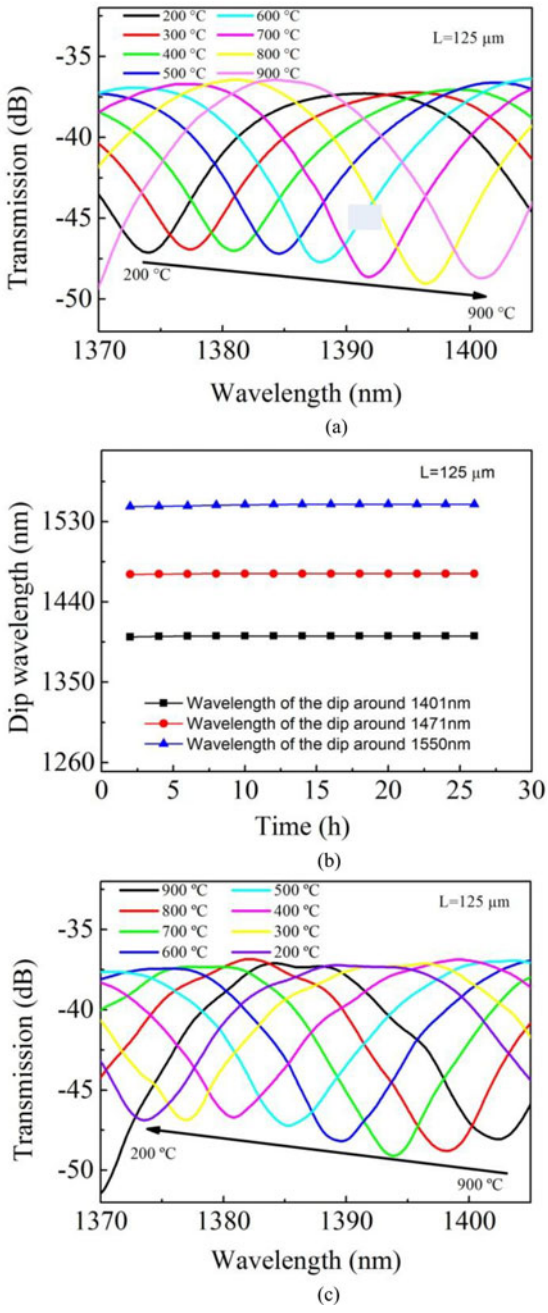

Fig. 6. (a) Transmission spectrum evolution from 200 °C to 900 °C. (b) Wavelength of the interference minimum around 1401, 1471, and 1550 nm versus heating time at 900 °C, respectively. (c) Transmission spectrum evolution from 900 °C to 200 °C.

at 1530 nm can be calculated to be 41.9 pm/ °C, which agree well with our experimental results. Comparing with previously reported fiber temperature sensors, the HCF-based interferometer exhibits a high temperature sensitivity that is four times higher than that of the multimode-fiber-based interferometer [19]–[21], and an excellent temperature stability that is much better than that of traditional FBGs [3]–[5]. In addition, this configuration is immune to external RI that is irrealizable for LPFG temperature sensors [15]–[18].

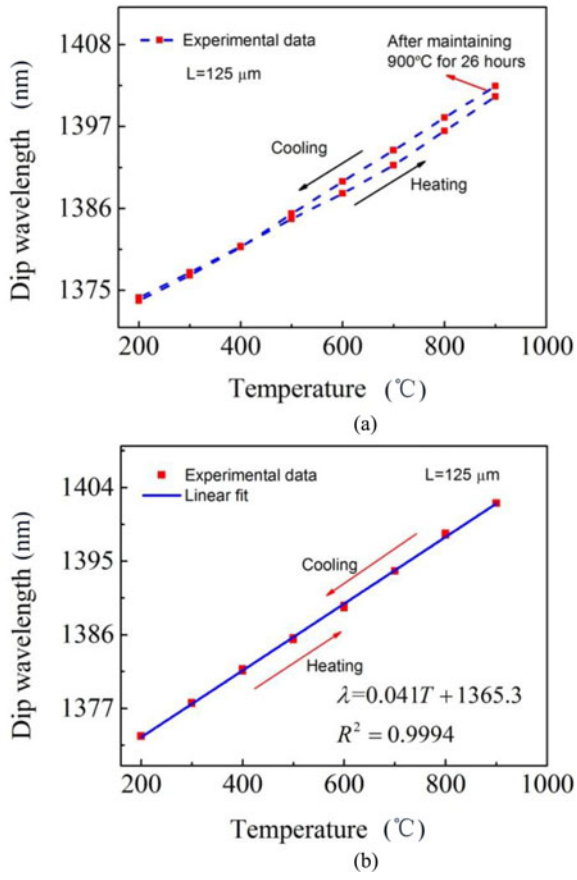

Fig. 7. Plot of indicated wavelength versus temperature in both heating and cooling process before (a) and after (b) three cycles annealing.

Table I
Refractive Index vs. Temperature, Fused Silica [25]

λ Microns	n 26 °C	n 471 °C	(d n/d T) / °C × 10^6	n 828 °C	(d n/d T) / °C × 10^6
0.5780	1.45899	1.46429	+11.9	1.46870	+12.1
1.12866	1.44903	1.45426	+11.8	1.45820	+11.4
1.36728	1.44635	1.45140	+11.4	1.45549	+11.4
1.52925	1.44444	1.44961	+11.6	1.45352	+11.3
1.660	1.44307	1.44799	+11.1	1.45174	+10.8

6. Conclusion

We demonstrate a robust optical fiber interferometric high-temperature sensor employing a SMF-HCF-SMF configuration that yields stable and repeatable measurements at a temperature up to 900 °C with no cross-sensitivity to external RI. The distinct thermo-optic coefficients between silica and air result in a relative high temperature sensitivity of 41 pm/ °C. The proposed sensor which is immune to the external RI may find vital applications in the fields of hyperthermal liquid temperature monitor.

References

[1] Y. J. Rao, "In-fibre Bragg grating sensors," *Meas. Sci. Technol.*, vol. 8, pp. 355–375, Apr. 1997.
[2] B. Lee, "Review of the present status of optical fiber sensors," *Opt. Fiber Technol.*, vol. 9, pp. 57–79, Apr. 2003.
[3] A. Othonos, "Fiber Bragg gratings," *Rev. Sci. Instrum.*, vol. 68, pp. 4309–4341, 1997.
[4] Z. Yang, H. Xu, and X. Dong, "Research development of high-temperature resistant fiber gratings," *Laser Optoelectron. Prog.*, vol. 49, pp. 050003-1–050003-8, 2012.
[5] I. Bennion, J. A. R. Williams, L. Zhang, K. Sugden, and N. J. Doran, "UV-written in-fibre Bragg gratings," *Opt. Quantum Electron.*, vol. 28, pp. 93–135, Feb. 1996.
[6] C. Liao and D. Wang, "Review of femtosecond laser fabricated fiber Bragg gratings for high temperature sensing," *Photon. Sens.*, vol. 3, pp. 97–101, 2013.
[7] C. M. Jewart, Q. Wang, J. Canning, D. Grobnic, S. J. Mihailov, and K. P. Chen, "Ultrafast femtosecond-laser-induced fiber Bragg gratings in air-hole microstructured fibers for high-temperature pressure sensing," *Opt. Lett.*, vol. 35, pp. 1443–1445, May 1, 2010.
[8] C. W. Smelser, S. J. Mihailov, and D. Grobnic, "Formation of type I-IR and type II-IR gratings with an ultrafast IR laser and a phase mask," *Opt. Exp.*, vol. 13, pp. 5377–5386, Jul. 2005.
[9] S. J. Mihailov *et al.*, "Fiber Bragg gratings made with a phase mask and 800-nm femtosecond radiation," *Opt. Lett.*, vol. 28, pp. 995–997, Jun. 2003.
[10] R. Yun-Jiang, W. Yi-Ping, R. Zeng-Ling, and Z. Tao, "Novel fiber-optic sensors based on long-period fiber gratings written by high-frequency CO_2 laser pulses," *J. Lightw. Technol.*, vol. 21, no. 5, pp. 1320–1327, May 2003.
[11] Y. Wang, "Review of long period fiber gratings written by CO_2 laser," *J. Appl. Phys.*, vol. 108, p. 081101, Oct. 15, 2010.
[12] X. W. Shu, T. Allsop, B. Gwandu, L. Zhang, and I. Bennion, "High-temperature sensitivity of long-period gratings in B-Ge codoped fiber," *IEEE Photon. Technol. Lett.*, vol. 13, no. 8, pp. 818–820, Aug. 2001.
[13] Y. J. Rao, Z. L. Ran, X. Liao, and H. Y. Deng, "Hybrid LPFG/MEFPI sensor for simultaneous measurement of high-temperature and strain," *Opt. Exp.*, vol. 15, pp. 14936–14941, Oct. 2007.
[14] Q. Han *et al.*, "Long-period grating inscribed on concatenated double-clad and single-clad fiber for simultaneous measurement of temperature and refractive index," *IEEE Photon. Technol. Lett.*, vol. 24, no. 13, pp. 1130–1132, Jul. 2012.
[15] Y. Huang, B. Chen, G. Chen, H. Xiao, and S. U. Khan, "Simultaneous detection of liquid level and refractive index with a long-period fiber grating based sensor device," *Meas. Sci. Technol.*, vol. 24, Sep. 2013, Art. no. 095303.
[16] T. Zhu, Y. J. Rao, J. L. Wang, and Y. Song, "A highly sensitive fiber-optic refractive index sensor based on an edge-written long-period fiber grating," *IEEE Photon. Technol. Lett.*, vol. 19, no. 24, pp. 1946–1948, Nov./Dec. 2007.
[17] M. N. Ng, Z. H. Chen, and K. S. Chiang, "Temperature compensation of long-period fiber grating for refractive-index sensing with bending effect," *IEEE Photon. Technol. Lett.*, vol. 14, no. 3, pp. 361–362, Mar. 2002.
[18] K. S. Chiang, Y. Q. Liu, M. N. Ng, and X. Y. Dong, "Analysis of etched long-period fibre grating and its response to external refractive index," *Electron. Lett.*, vol. 36, pp. 966–967, May 2000.
[19] L. Enbang, W. Xiaolin, and Z. Chao, "Fiber-optic temperature sensor based on interference of selective higher-order modes," *Appl. Phys. Lett.*, vol. 89, pp. 91119-1–91119-3, Aug. 28, 2006.
[20] L. Yu and W. Li, "Low-cost high-sensitivity strain and temperature sensing using graded-index multimode fibers," *Appl. Opt.*, vol. 46, pp. 2516–2519, May 1, 2007.
[21] L. V. Nguyen, D. Hwang, S. Moon, D. S. Moon, and Y. Chung, "High temperature fiber sensor with high sensitivity based on core diameter mismatch," *Opt. Exp.*, vol. 16, pp. 11369–11375, Jul. 21, 2008.
[22] Y. Wang, M. W. Yang, D. N. Wang, S. J. Liu, and P. X. Lu, "Fiber in-line Mach-Zehnder interferometer fabricated by femtosecond laser micromachining for refractive index measurement with high sensitivity," *J. Opt. Soc. Amer. B, Opt. Phys.*, vol. 27, pp. 370–374, Mar. 2010.
[23] Y. Wang, Y. H. Li, C. R. Liao, D. N. Wang, M. W. Yang, and P. X. Lu, "High-temperature sensing using miniaturized fiber in-line Mach Zehnder interferometer," *IEEE Photon. Technol. Lett.*, vol. 22, no. 1, pp. 39–41, Jan. 2010.
[24] T. Y. Hu, Y. Wang, C. R. Liao, and D. N. Wang, "Miniaturized fiber in-line Mach–Zehnder interferometer based on inner air cavity for high-temperature sensing," *Opt. Lett.*, vol. 37, pp. 5082–5084, 2012.
[25] J. H. Wray and J. T. Neu, "Refractive index of several glasses as a function of wavelength and temperature," *J. Opt. Soc. Amer.*, vol. 59, pp. 774–776, 1969.
[26] B. Kuhn and R. Schadrack, "Thermal expansion of synthetic fused silica as a function of OH content and fictive temperature," *J. Non-Cryst. Solids*, vol. 355, pp. 323–326, Feb. 2009.